Supplemental material

Supplemental discussion of internal OH and its possible removal by C_3F_6 addition

OHchem represents the real OH and OHwave-OHchem represents an instrument interference only if no internal OH is removed when C_3F_6 is added. This can be seen in the following analysis.

The total detected OH by wavelength modulation is the sum of ambient OH ($OH_{ambient}$) and internal OH ($OH_{internal}$), whereas OH detected by chemical removal is the sum of the ambient OH and the fraction of internal OH that is removed. So

$$OH_{wave} = OH_{ambient} + OH_{internal}$$

$$OH_{chem} = OH_{ambient} + (1-\alpha)OH_{internal}$$

where α is the fraction of internal produced OH remaining from the external addition of C_3F_6. Assuming

$$x = \frac{OH_{chem}}{OH_{wave}}$$

The relationship between $OH_{ambient}$ and OH_{wave} can then be described as

$$f = \frac{OH_{ambient}}{OH_{chem}} = \frac{\alpha + x - 1}{\alpha x}$$

For α = 1, f = 1 and $OH_{chem} = OH_{ambient,}$ no matter what x is. For α = 0.8, when x = 0.4, f 0.63, and when x=0.5, f=0.75. This analysis suggests that the ambient OH equals .63 to 1 times OH_{chem}, depending on where the internal OH is being generated. The question then is "Where is the internal OH being generated?"

A key to determining the source of the internal OH is the removal from OH generated by Hg lamps 1, 2, and 3 by the addition of different amounts of C_3F_6 (Zhang et al., manuscript in preparation). The shapes of the three removal curves are very different, with the shape of the removal more curved for external OH, less curved for OH produced near the inlet (Hg lamp 2) and small but slowly increasing for OH produced in the detection axis (Hg lamp 3). If OH were generated near the inlet, the ratio of OHchem to OHwave would go to less than 10% as more C_3F_6 was added because both external OH and internal OH generated near the inlet are effectively removed when more than 4 sccm of C_3F_6 were added. If OH were generated in the detection axis, the OHchem to OHwave

effectively levels off because most of the external OH is removed while little of the internal OH is. The curve of OH produced from ozone and MBO or β-pinene matches a curve that combines curves with about 50% from external OH, 14% from internal OH generated near the inlet, and 36% from OH generated in the detection axis. Applying the laboratory-derived remaining internal OH, α, (0.83±0.08) to the BEARPEX09-observed average OHchem/OHwave (0.50), the equation for $OH_{ambient}/OH_{chem}$ equals 0.80±0.12. We apply this correction to OHchem but retain the name "OHchem" for this corrected value. Because we have quantified the internal OH loss and corrected OHchem for it, OHchem is a quantitative measure of the real OH.

Model mechanism tests

The base photochemical box model uses the Regional Atmospheric Chemistry Mechanism, Version 2 (RACM2) mechanism (Henderson et al., 2011). The "RACM2 + IEPOX" scheme was modified by replacing isoprene oxidation in RACM2 with the isoprene nitrate chemistry described in Paulot et al. (2009a) and the isoprene epoxide chemistry in Paulot et al. (2009b). The "RACM2 + IEPOX + Isomerization" scheme was modified based on "RACM2 + IEPOX", by adding the unimolecular isomerization mechanism described by Peeters et al. (Peeters et al., 2009) and Peeters and Müller (2010). The "RACM2 + IEPOX + Reduced Isomerization" was modified based on "RACM2 + IEPOX + Isomerization", by using the reduced rate of isomerization for isoprene hydroxylperoxy radicals suggested by Crounse et al. (Crounse et al., 2011). The MBO oxidation was explicitly treated in "RACM2 + IEPOX", "RACM2 + IEPOX + Isomerization" and "RACM2 + IEPOX + Reduced Isomerization", following Carrasco et al. (2007), Steiner et al. (2007), and Chan et al. (2009). Photooxidation of monoterpenes and sesquiterpenes was based on Wolfe and Thornton (2011). Photolysis rates were calculated by the Tropospheric Ultraviolet and Visible (TUV) radiation model and then scaled based on the Photosynthetically Active Radiation (PAR) measurements.

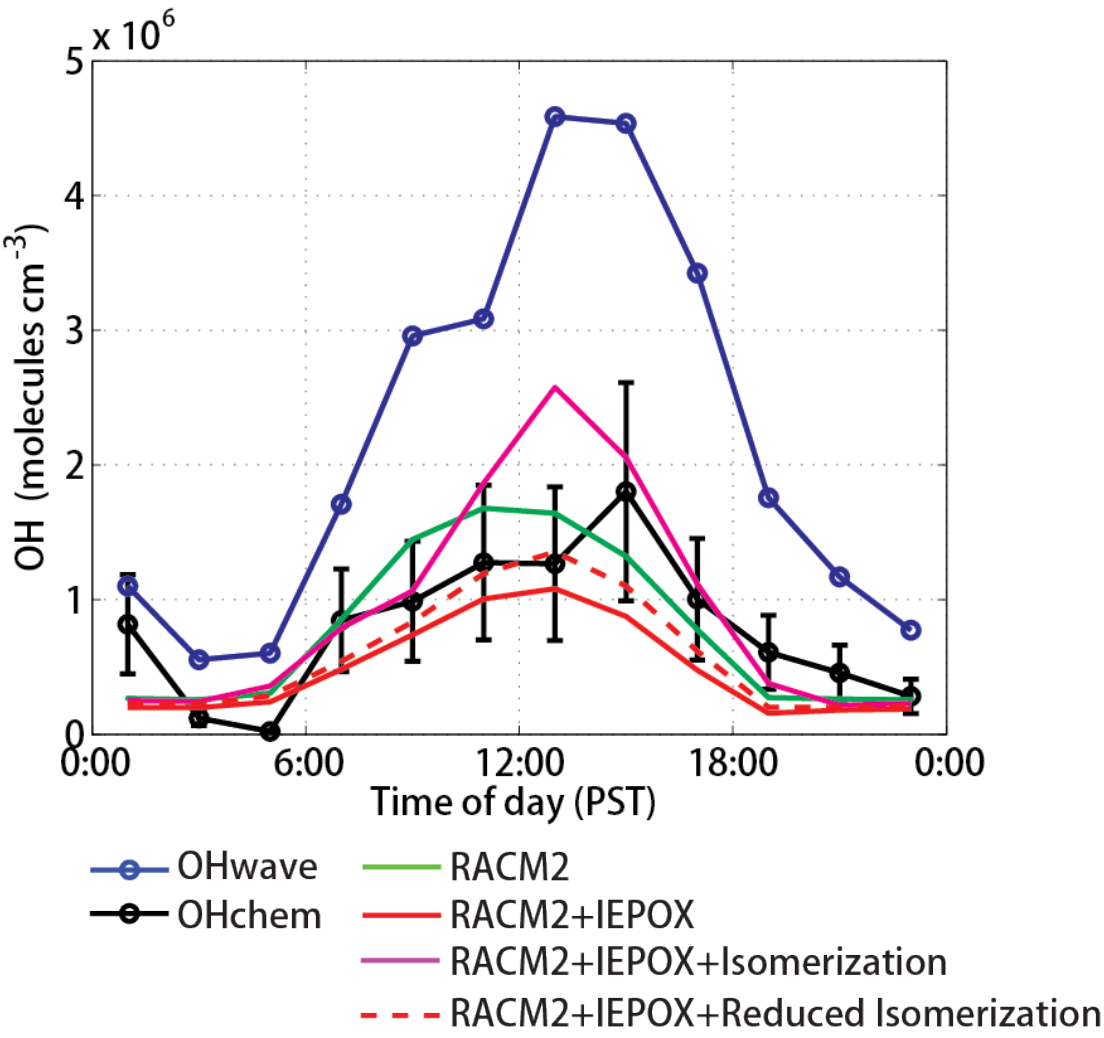

Figure S1. Diurnal cycle of measured and modeled OH between 20 June and 30 July 2009 near the Blodgett Forest Research Station (BFRS). "OHwave" is represented by blue open circles and "OHchem" by black open circles. The vertical bars indicate OHchem's absolute uncertainty of ±45% (2σ confidence), which comes from combining the uncertainty from the internally generated OH is removed by the C_3F_6 addition used to measure OHchem (±20%) and the absolute uncertainty of the OH measurements (±40% at 2σ confidence). Note that OHchem here is corrected by 0.80 to account for the removal of internal OH by C_3F_6 addition. Model results are shown as the base RACM2 model (green solid lines), the "RACM2 + IEPOX" scheme (red solid lines), the "RACM2 + IEPOX + Isomerization" scheme (magenta solid lines), and the "RACM2 + IEPOX + Reduced Isomerization" scheme (red dashed lines) (see text for details). Note that the "RACM2 + IEPOX + Reduced Isomerization" scheme is identical to the simulation used in the main text.

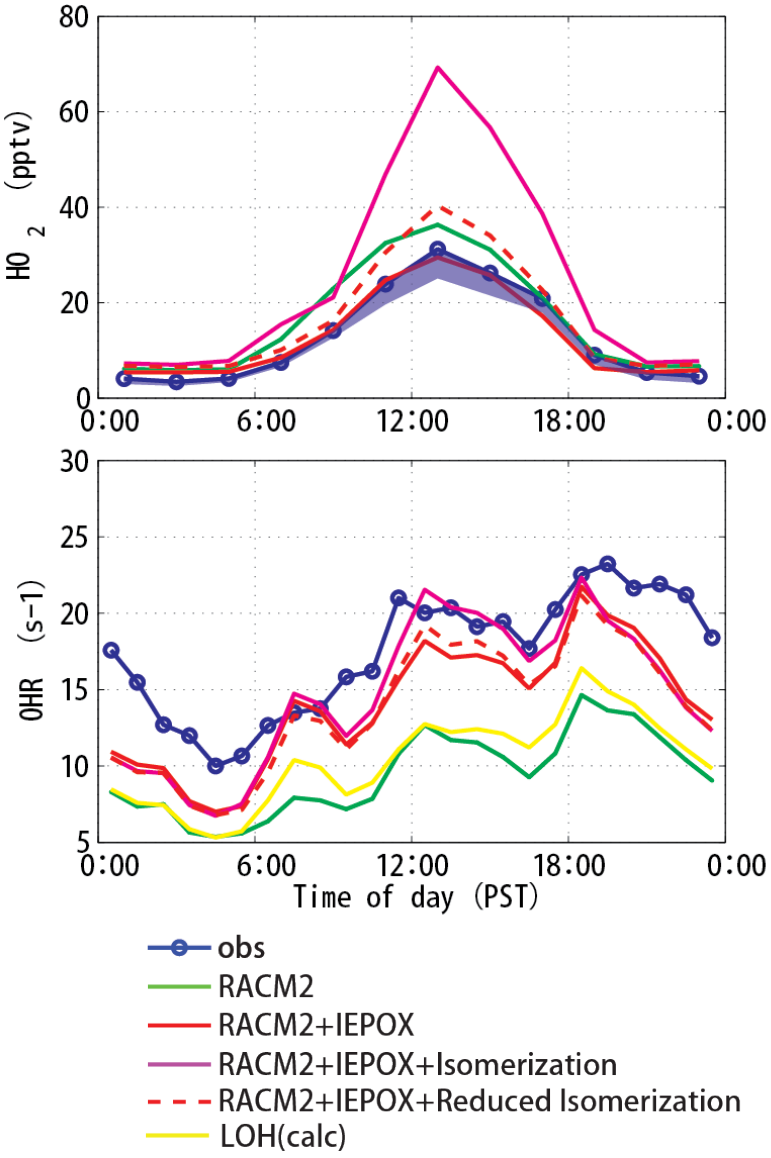

Figure S2. Diurnal cycle of HO_2 (top panel) and OH reactivity (bottom panel) between 20 June and 30 July 2009 near the Blodgett Forest Research Station (BFRS). In the top panel, the shaded area below measured HO_2 (blue open circles) indicates the contribution to measured HO_2 from an RO_2 interference from isoprene, MVK and MACR (Fuchs et al., 2011). In the bottom panel, the calculated OH reactivity from available measurements (LOH) is represented by a yellow line. Model results are shown as the base RACM2 model (green solid lines), the "RACM2 + IEPOX" scheme (red solid lines), the "RACM2 + IEPOX + Isomerization" scheme (magenta solid lines), and the "RACM2 + IEPOX + Reduced Isomerization" scheme (red dashed lines) (see text for details). Note that the "RACM2 + IEPOX + Reduced Isomerization" scheme is identical to the simulation used in the main text. The discrepancy between LOH and RACM2 is mainly due to the species lumping.

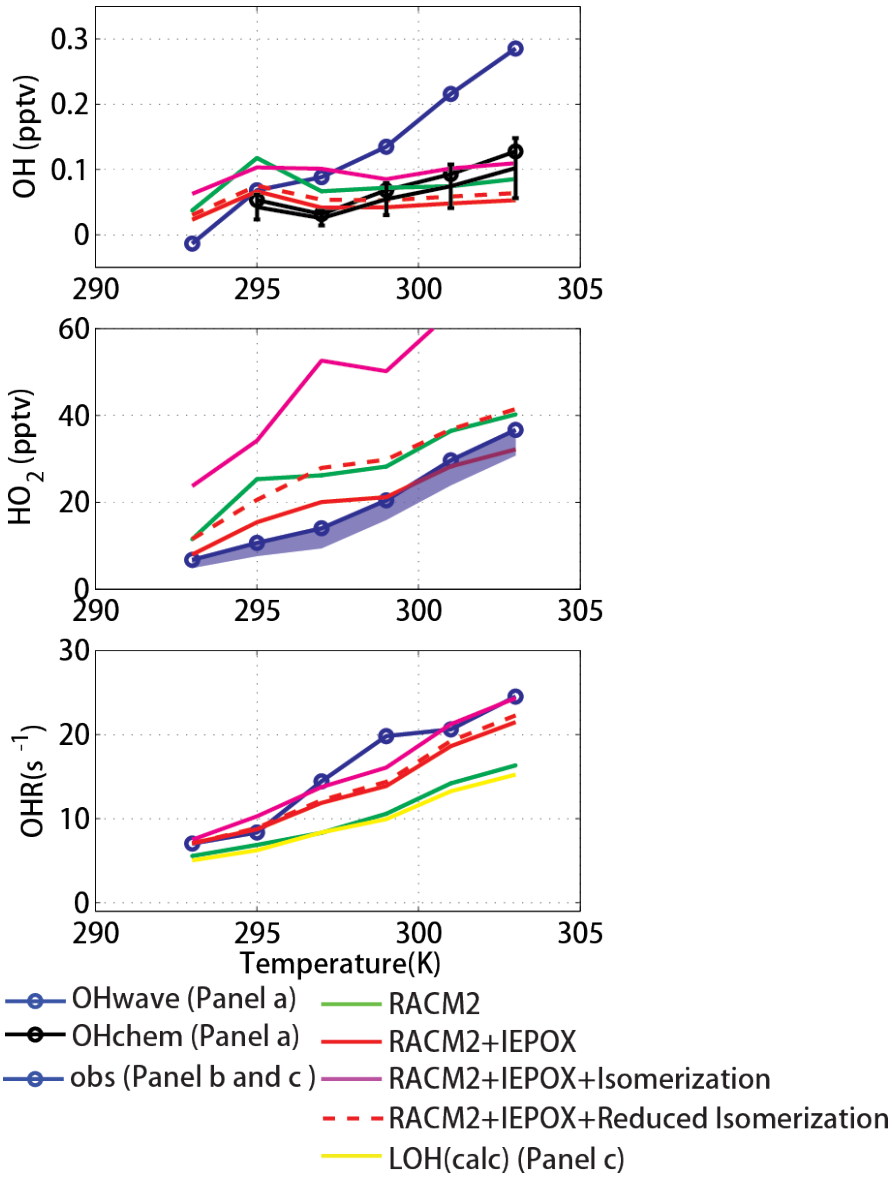

Figure S3 Temperature dependence of (a) daytime measured and modeled OH, (b) daytime measured and modeled HO_2, and (c) OH reactivity between 9:00 and 15:00 PST during BEARPEX09. In panel (a), "OHwave" is represented by blue open circles and "OHchem" by black open circles. The vertical bars indicate a combined uncertainty (±45%) from the internally generated OH is removed by the C_3F_6 addition used to measure OHchem (20%), and the absolute uncertainty of the OH measurements (±40% at 2σ confidence). In panel (b), the shaded area below measured HO_2 (blue open circles) indicates the contribution to measured HO_2 from a RO_2 interference from isoprene, MVK and MACR (Fuchs et al., 2011). In panel (c), the calculated OH reactivity from available measurements is represented by a yellow line. Model results are shown as the base RACM2 model (green solid lines), the "RACM2 + IEPOX" scheme (red solid lines), the

“RACM2 + IEPOX + Isomerization” scheme (magenta solid lines), and the “RACM2 + IEPOX + Reduced Isomerization” scheme (red dashed lines) (see text for details). Note that the “RACM2 + IEPOX + Reduced Isomerization” scheme is identical to the simulation used in the main text.

Table S1 Other measured species and their averaged concentrations (Unit: pptv) [a]

Species	Daytime Conc (9am-3pm)	24h average	Measured by	Height
Glyoxal	64 ± 33	65 ± 36	Laser-Induced Phosphorescence	2m, 3m, 9m ,18m
HCHO	4300 ± 2200	4600 ± 2300	Laser-Induced Fluorescence	2m, 3m, 9m ,18m
Glycolaldehyde	1110 ± 694	1108 ± 673	CIMS	18m
H_2O_2	1105 ± 348	822 ± 396	CIMS	18m
Hydroxyacetone	697 ± 460	760 ± 460	CIMS	18m
Acetone	3300 ± 1300	3600 ± 1300	GC-FID/PTR-MS	2, 6, 10, 14, 18m
Acetonitrile	150 ± 50	160 ± 50	PTR-MS	2, 6, 10, 14, 18m
Acetaldehyde	1500 ± 800	1900 ± 1000	PTR-MS	2, 6, 10, 14, 18m
α-Pinene	100 ± 60	210 ± 160	GC-FID	18m
β-Pinene	70 ± 40	130 ± 90	GC-FID	18m
Butane	160 ± 180	170 ± 190	GC-FID	18m
Butanol	3100 ± 800	3700 ± 1300	GC-FID	18m
Camphene	9.4 ± 6.7	13 ± 9.6	GC-FID	18m
Isobutylalcohol	120 ± 60	130 ± 50	GC-FID	18m
Isoprene	1700 ± 800	1.4 ± 0.7) × 10^3	GC-FID	18m
MVK	570 ± 400	540 ± 390	GC-FID/PTR-MS	18m
MACR	220 ± 160	230 ± 160	GC-FID/PTR-MS	18m
MBO	3000 ± 1600	2200 ± 1900	GC-FID/PTR-MS	2, 6, 10, 14, 18m
Sum of Sesquiterpenes	62 ± 44	83 ± 68	PTR-MS	2, 6, 10, 14, 18m
MethylChavicol	62 ± 40	98 ± 90	PTR-MS	2, 6, 10, 14, 18m
Methanol	13700 ± 5400	16300 ± 8100	PTR-MS	2, 6, 10, 14, 18m
Ethanol	1700 ± 700	800 ± 700	GC-FID	18m
Benzene	48 ± 31	62 ± 40	PTR-MS	2, 6, 10, 14, 18m
Toluene	195 ± 129	253 ± 185	GC-FID	18m
HNO_3	330 ± 20	320 ± 60	TD-LIF	18m
MPAN	29 ± 15	19 ± 15	CIMS	1,2 ,6, 10, 14, 18m
PAN	275 ± 199	248 ± 171	CIMS	1,2 ,6, 10, 14, 18m
PPN	15 ± 16	13 ± 16	CIMS	1,2 ,6, 10, 14,

				18m
NO_2[b]	200 ± 200	800 ± 3300	TD-LIF	1, 4, 9, 18 m
NO[b]	74 ± 240	300 ± 4300	Chemiluminescence	1, 4, 9, 18 m
HONO	15 ± 10	33 ± 31	Wet chemistry	14 m
CO	(130 ± 28) × 10^3	(137 ± 29) × 10^3	TECO 48C	12.5 m
O_3	(54 ± 8) × 10^3	(53 ± 11) × 10^3	Dasibi 1008-PC Ozone Analyzers	2, 6, 10, 14, 18m

[a] Total alkyl nitrates are not included due to the lack of detailed speciation.

[b] NO and NO_2 were influenced by generator plumes at night.

Table S2 OH yield from ozonolysis of terpenes

Species	Yield	Reference
β-caryophyllene (C15H24)	0.16 ± 0.4	Winterhalter et al. (2009)
Camphene	<0.18	Atkinson et al. (1992)
2-Carene	0.81 ± 0.11	Aschmann et al. (2002)
3-Carene	0.86 ± 0.11	Aschmann et al. (2002)
Limonene	0.67 ± 0.10	Aschmann et al. (2002)
Myrcene	0.63 ± 0.09	Aschmann et al. (2002)
β-Phellandrene	0.14	Atkinson et al. (1992)
α-Pinene	0.77 ± 0.10	Aschmann et al. (2002)
β-Pinene	0.35	Atkinson et al. (1992)
Ocimene	0.55 ± 0.09	Atkinson et al. (1992)
Sabinene	0.33 ± 0.05	Atkinson et al. (1992)
α-Terpinene	0.38 ± 0.05	Aschmann et al. (2002)
γ-Terpinene	0.81 ± 0.11	Aschmann et al. (2002)
Terpinolene	0.74 ± 0.10	Atkinson et al. (1992)
Linalool	0.66 ± 0.10	Atkinson et al. (1995)
α -Phellandrene	0.34 ± 0.08	Herrmann et al. (2010)

Reference

Aschmann, S. M., Arey, J., and Atkinson, R.: OH radical formation from the gas-phase reactions of O-3 with a series of terpenes, Atmos. Environ., 36, 4347-4355, 2002.

Atkinson, R., Aschmann, S. M., Arey, J., and Shorees, B.: Formation of OH Radicals in the Gas Phase Reactions of O3 With a Series of Terpenes, J. Geophys. Res., 97, 6065-6073, 10.1029/92jd00062, 1992.

Atkinson, R., Arey, J., Aschmann, S. M., Corchnoy, S. B., and Shu, Y.: Rate constants for the gas-phase reactions of cis-3-Hexen-1-ol, cis-3-Hexenylacetate, trans-2-Hexenal, and Linalool with OH and NO3 radicals and O3 at 296 ± 2 K, and OH radical formation yields from the O3 reactions, Int. J. Chem. Kinet., 27, 941-955, 10.1002/kin.550271002, 1995.

Carrasco, N., Doussin, J. F., O'Connor, M., Wenger, J. C., Picquet-Varrault, B., Durand-Jolibois, R., and Carlier, P.: Simulation chamber studies of the atmospheric oxidation of 2-methyl-3-buten-2-ol: Reaction with hydroxyl radicals and ozone under a variety of conditions, J. Atmos. Chem., 56, 33-55, 10.1007/s10874-006-9041-y, 2007.

Chan, A. W. H., Galloway, M. M., Kwan, A. J., Chhabra, P. S., Keutsch, F. N., Wennberg, P. O., Flagan, R. C., and Seinfeld, J. H.: Photooxidation of 2-Methyl-3-Buten-2-ol as a Potential Source of Secondary Organic Aerosol (vol 43, pg 4647, 2009), Environ. Sci. Technol., 43, 8470, 10.1021/es902789a, 2009.

Crounse, J. D., Paulot, F., Kjaergaard, H. G., and Wennberg, P. O.: Peroxy radical isomerization in the oxidation of isoprene, PCCP Phys. Chem. Chem. Phys., 2011.

Fuchs, H., Bohn, B., Hofzumahaus, A., Holland, F., Lu, K. D., Nehr, S., Rohrer, F., and Wahner, A.: Detection of HO2 by laser-induced fluorescence: calibration and interferences from RO2 radicals, Atmos. Meas. Tech., 4, 1209-1225, 10.5194/amt-4-1209-2011, 2011.

Henderson, B. H., Pinder, R. W., Crooks, J., Cohen, R. C., Hutzell, W. T., Sarwar, G., Goliff, W. S., Stockwell, W. R., Fahr, A., Mathur, R., Carlton, A. G., and Vizuete, W.: Evaluation of simulated photochemical partitioning of oxidized nitrogen in the upper troposphere, Atmos. Chem. Phys., 11, 275-291, 10.5194/acp-11-275-2011, 2011.

Herrmann, F., Winterhalter, R., Moortgat, G. K., and Williams, J.: Hydroxyl radical (OH) yields from the ozonolysis of both double bonds for five monoterpenes, Atmos. Environ., 44, 3458-3464, 10.1016/j.atmosenv.2010.05.011, 2010.

Paulot, F., Crounse, J. D., Kjaergaard, H. G., Kroll, J. H., Seinfeld, J. H., and Wennberg, P. O.: Isoprene photooxidation: new insights into the production of acids and organic nitrates, Atmos. Chem. Phys., 9, 1479-1501, 2009a.

Paulot, F., Crounse, J. D., Kjaergaard, H. G., Kurten, A., St Clair, J. M., Seinfeld, J. H., and Wennberg, P. O.: Unexpected Epoxide Formation in the Gas-Phase Photooxidation of Isoprene, Science, 325, 730-733, 10.1126/science.1172910, 2009b.

Peeters, J., Nguyen, T. L., and Vereecken, L.: HOx radical regeneration in the oxidation of isoprene, PCCP Phys. Chem. Chem. Phys., 11, 5935-5939, 10.1039/b908511d, 2009.

Peeters, J., and Müller, J. F.: HOx radical regeneration in isoprene oxidation via peroxy radical isomerisations. II: experimental evidence and global impact, PCCP Phys. Chem. Chem. Phys., 12, 14227-14235, 10.1039/c0cp00811g, 2010.

Steiner, A. L., Tonse, S., Cohen, R. C., Goldstein, A. H., and Harley, R. A.: Biogenic 2-methyl-3-buten-2-ol increases regional ozone and HOx sources, Geophys. Res. Lett., 34, 10.1029/2007gl030802, 2007.

Winterhalter, R., Herrmann, F., Kanawati, B., Nguyen, T. L., Peeters, J., Vereecken, L., and Moortgat, G. K.: The gas-phase ozonolysis of beta-caryophyllene (C15H24). Part I: an experimental study, PCCP Phys. Chem. Chem. Phys., 11, 4152-4172, 10.1039/b817824k, 2009.

Wolfe, G. M., and Thornton, J. A.: The Chemistry of Atmosphere-Forest Exchange (CAFE) Model – Part 1: Model description and characterization, Atmos. Chem. Phys., 11, 77-101, 10.5194/acp-11-77-2011, 2011.